Dynamic Oxygen Challenge Evaluated by NMR T_1 and T_2^* – insights into tumor oxygenation

Dawen Zhao[#1], **Jesús Pacheco-Torres**[#1,2,∞], **Rami R. Hallac**[1], **Derek White**[1], **Peter Peschke**[3], **Sebastian Cerdán**[2], and **Ralph P. Mason**[1,¥]

[1] Department of Radiology, University of Texas Southwestern Medical Center, Dallas, Texas, USA 75390

[2] Laboratory for Imaging and Spectroscopy by Magnetic Resonance LISMAR, Instituto de Investigaciones Biomédicas "Alberto Sols" CSIC/UAM, Arturo Duperier 4, Madrid 28029, Spain.

[3] Clinical Cooperation Unit Molecular Radiooncology, German Cancer Research Center (DKFZ), Heidelberg, Germany

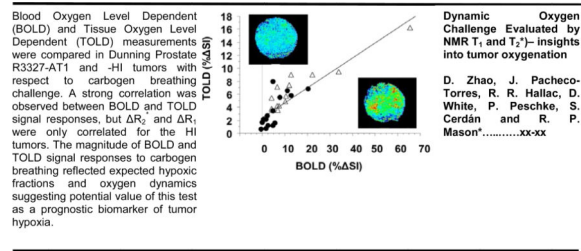[#] These authors contributed equally to this work.

Abstract

There is intense interest in developing non-invasive prognostic biomarkers of tumor response to therapy, particularly with regard to hypoxia. It has been suggested that oxygen sensitive MRI, notably Blood Oxygen Level Dependent (BOLD) and Tissue Oxygen Level Dependent (TOLD) may provide relevant measurements. This study examined the feasibility of interleaved T_2^*- and T_1-weighted oxygen sensitive MRI, as well as R_2^* and R_1 maps of rat tumors to assess the relative sensitivity to changes in oxygenation. Investigations used cohorts of Dunning Prostate R3327-AT1 and -HI tumors, which are reported to exhibit distinct size-dependent levels of hypoxia and response to hyperoxic gas breathing. Proton MRI R_1 and R_2^* maps were obtained for tumors of anesthetized rats (isoflurane/air) at 4.7 T. Then, interleaved gradient echo T_2^*- and T_1-weighted images were acquired during air breathing and a ten minute challenge with carbogen (95% O_2/5% CO_2).

Signals were stable during air breathing and each type of tumor showed distinct signal response to carbogen. T_2^* (BOLD) response preceded T_1 (TOLD) responses, as expected. Smaller HI tumors (reported to be well oxygenated) showed the largest BOLD and TOLD responses. Larger AT1 tumors (reported to be hypoxic and resist modulation by gas breathing) showed the smallest response. There was a strong correlation between BOLD and TOLD signal responses, but R_2^* and R_1 were only correlated for the HI tumors. The magnitude of BOLD and TOLD signal responses to carbogen breathing reflected expected hypoxic fractions and oxygen dynamics suggesting potential value of this test as a prognostic biomarker of tumor hypoxia.

Graphical Abstract

[¥]To whom correspondence should be addressed: Ralph P. Mason, PhD Department of Radiology UT Southwestern Medical Center 5323 Harry Hines Blvd. Dallas, TX 75390-9058 USA Phone: +1 (214) 648-8926 Fax: +1 (214) 648-2991 Ralph.Mason@UTSouthwestern.edu.
[∞]Current address: Cellular and Systems Neurobiology Unit, Instituto de Neurociencias, Consejo Superior de Investigaciones Científicas & Universidad Miguel Hernández, Sant Joan d'Alacant 03550, Spain

Blood Oxygen Level Dependent (BOLD) and Tissue Oxygen Level Dependent (TOLD) measurements were compared in Dunning Prostate R3327-AT1 and -HI tumors with respect to carbogen breathing challenge. A strong correlation was observed between BOLD and TOLD signal responses, but ΔR_2^* and ΔR_1 were only correlated for the HI tumors. The magnitude of BOLD and TOLD signal responses to carbogen breathing reflected expected hypoxic fractions and oxygen dynamics suggesting potential value of this test as a prognostic biomarker of tumor hypoxia.

Dynamic Oxygen Challenge Evaluated by NMR T_1 and T_2^*– insights into tumor oxygenation

D. Zhao, J. Pacheco-Torres, R. R. Hallac, D. White, P. Peschke, S. Cerdán and R. P. Mason*............xx-xx

Keywords

INTRODUCTION

Tumor hypoxia is widely reported to influence response to therapy. Moreover, hypoxia has been linked to tumor aggressiveness resulting from stress induced genetic instability, stimulated angiogenesis and metastatic tendency (1). The fundamental studies of Gray *et al.* demonstrated the influence of hypoxia on response to radiation (2). More recently, polarographic electrode measurements of pO_2 distributions and hypoxic fractions in patients confirmed poor outcome for hypoxic tumors in several disease sites including prostate (1, 3).

Stratifying patient tumors based on hypoxia is particularly timely since there are increasing opportunities to tailor therapy to tumor characteristics, potentially enhancing success through personalized medicine. Thus, there is a true need for prognostic biomarkers to identify hypoxia in human tumors and many diverse modalities and reporter molecules are under evaluation (1, 4, 5). Based on oxygen electrode measurements Movsas *et al.* showed poorer outcome in terms of locoregional control and distant metastasis in men with hypoxic prostate cancer (3). Vergis *et al.* found that biochemical failure was significantly more prevalent for men with elevated HIF1-α, VEGF and osteopontin expression in biopsy samples (6).

Oxygen sensitive MRI is attractive, since it is non-invasive and avoids the need for an exogenous reporter agent. Increasingly, reports suggest the feasibility of Blood Oxygen Level Dependent (BOLD) and Tissue Oxygen Level Dependent (TOLD) contrast MRI in patients (7-14). BOLD effects have been evaluated in numerous pre-clinical tumor types in animal models and several studies have demonstrated a correlation with measurements of pO_2 based on polarographic electrodes (15, 16), fluorescent fiber optic probes (17), ESR (18, 19) and ^{19}F MRI (20, 21). Others have examined consistency with immunohistochemical markers such as hypoxia, and vascular extent (22, 23).

BOLD MRI is sensitive to changes in deoxyhemoglobin concentration, but it is also influenced by vascular volume, flow, microvessel diameter and consequent transit ability of red blood cells containing deoxyhemoglobin to (24-26). R_1 ($=1/T_1$) is sensitive to pO_2, since molecular oxygen is paramagnetic (27, 28). R_1 is subject to modulation by many parameters including ionic strength, metal ions, and potentially deoxyhemoglobin, so that R_1 is not expected to be directly correlated with pO_2 in tumors. With respect to a simple hyperoxic

gas challenge intervention many parameters such as ion and protein concentrations are expected to remain largely unchanged. A predicted TOLD effect was reported using hyperbaric (29) or hyperoxic oxygen breathing challenges (14). Recently, intense interest has developed in combining observations of both R_1 and R_2* in pre-clinical animal systems and patients (13, 30-33).

These reports prompted us to explore BOLD and TOLD measurements in response to carbogen breathing challenge in two rat prostate tumor types noted for differential growth rates, vascular development, oxygenation and radiation response (34, 35). Specifically, we examined differences in signal intensity in T_1- and T_2*-weighted images, as well as relaxation rates (R_1 and R_2*) with respect to carbogen breathing challenge.

EXPERIMENTAL

Investigations were approved by the Institutional Animal Care and Research Advisory Committee.

Tumor models

Two sublines of the Dunning prostate R3327 adenocarcinoma were selected based on extensive previous reports regarding differential hypoxia, response to hyperoxic gas challenge and response to radiation (34-38). The HI subline is moderately well-differentiated, hormone-insensitive and relatively slow growing with a tumor volume doubling time (VDT) of 9 days; while, the AT1 is a faster growing, poorly-differentiated subline with a VDT of 4.4 days (39). Pieces of freshly excised donor tumor tissue were implanted subcutaneously in the thigh of adult male Copenhagen rats (~250 g, Harlan, Indianapolis, IN), as described in detail previously (40). Typical histological characteristics are presented in Figure 1. Tumors were investigated by MRI when small (<3 cm^3) or large (>3 cm^3). Seventeen HI tumors, including 8 smaller (size range 0.7 – 2.6 cm^3) and 9 larger (range 3.6 – 7 cm^3), and 16 AT1 tumors, including 9 smaller (range 0.75 – 2.2 cm^3) and 7 larger (range 3.1 – 5.8 cm^3) were investigated.

MRI

MRI experiments were performed using a Varian Unity Inova® 4.7 T horizontal bore system (Agilent, Palo Alto, CA) equipped with actively shielded gradients. Each rat was maintained under general gaseous anesthesia (air and 1.5% isoflurane). The rat body temperature was maintained using a warm water blanket at about 36 °C, though not measured continuously. The tumor was placed inside a size-matched single-turn ^{1}H volume coil, which provided both transmit and receive functions. Following shimming on tissue water signal to a typical linewidth of 50 Hz, a spin echo multiple slice (SEMS) sequence was applied to acquire R_1 maps under air breathing (baseline) with acquisition parameters: repetition time (TR) arrayed as 9 values from 100 ms to 3.5 s, echo time (TE) = 20 ms, FOV = 40 × 40 mm, matrix = 64 × 64 and 3 adjacent slices each 1.5 mm thick and separated by 1 mm space in 10½ mins. Baseline R_2* maps were obtained with a gradient echo multiple slice (GEMS) sequence with 7 echoes (TR = 195 ms, initial TE = 7 ms and spacing = 6 ms, echo train duration = 42 ms, using the same spatial resolution as for R_1 maps) in 3 min. Then a series

of 5 T_1-weighted (TR = 30 ms, TE = 5 ms, flip angle = 45°; acquisition time = 3 s, matrix= 128x128) and T $*_2$-weighted (TR = 150 ms, TE = 20 ms, flip angle = 20°, acquisition time = 19 s, matrix= 128x128) spoiled gradient-echo images were acquired in an interleaved fashion, as baseline. At this point, the breathing gas was changed to carbogen (CB; 95% O_2 plus 5% CO_2 at 1 dm^3/min) and a series of 20 interleaved T_1- and T_2*-weighted images was acquired over 10 mins. Finally, R_1 and R $*_2$ values were measured again during CB inhalation.

Immunohistochemistry

Additional AT1 and HI tumors were implanted as above specifically for histological comparison based on published methods (36, 41). Briefly, when tumors reached about 1 cm diameter pimonidazole hydrochloride (Hypoxyprobe-1; NPI, Belmont, MA) was injected into the tail vein at a dose of 60 mg/kg. Ninety minutes later, rats were anesthetized and perfused for 20 minutes with physiological saline containing 5 mM $CaCl_2$. Tumors were resected from living rats, cut in half, and halves rapidly placed in liquid nitrogen or 10% formalin respectively. Monoclonal antibody Mab1 (NPI) that detects pimonidazole–protein adducts was added to frozen sections (8 μm) followed by incubation for 2 hours at 37 °C. Slides were then incubated for 1 hour at 37 °C with horseradish peroxidase (HRP)–conjugated goat antimouse secondary. After a PBST wash, sections were immersed in 3,3′-diaminobenzidine (DAB) in H_2O for 1 minute at room temperature to visualize HRP-enzyme activity. For H&E staining, tumor tissues were fixed in 10% formalin, embedded in paraffin, and sectioned (4 μm).

Data analysis

Data analysis was performed using IDL-based software. Signal Intensity (SI) in the initial five T_1- or T_2*-weighted images (during air breathing) was averaged to obtain mean baseline images and relative changes in signal intensity with respect to CB challenge were calculated on a voxel by voxel basis. R_1 values for a given voxel were obtained by fitting the signal intensities corresponding to 9 delay values to a three-parameter least squares curve, using a Levenberg-Marquardt algorithm. R_2* values for a given voxel were obtained by fitting an exponential model of signal decay curve. Common voxels (typically, 1,300 to 2,500 depending on tumor size) were compared under carbogen and air breathing and differences calculated: $R_{1 \text{ or } 2*} = (R_{1 \text{ or } 2*}^{CB} - R_{1 \text{ or } 2*}^{air})$.

Statistical analysis

Statistical significance of changes in signal intensity in T_1- and T_2*-weighted images and relaxation rates was assessed using one way analysis of variance (ANOVA) and Fisher's PLSD (Protected Least Significant Difference) or Student's t-tests. Data are presented as mean ± standard error (SE).

RESULTS

Considerable spatial heterogeneity was observed during air breathing (baseline), particularly in T_2*-weighted MR images, but signal intensity was generally stable (mean SI in T_2*- and T_1-weighted images being less than 1%, Figs. 2-5). Increased signal intensity in T_2*-

weighted images was significant within 30 seconds of switching gases in 12 of 13 HI tumors and 13 of 16 AT1 tumors irrespective of size. Within two minutes signal reached a stable plateau for both smaller (8 of 8) and larger (3 of 5) HI tumors and smaller (6 of 9) AT1 tumors (Figs. 2-4 a-c). Larger AT1 tumors sometimes showed a transient increase with return to baseline after two to six minutes (4 of 7) (Fig. 5c). Response to carbogen was heterogeneous with focal signal changes ranging from plus 100% to minus 40%, but the mean value for each adjacent slice was quite uniform (Figs. 2-5 c). T_1-weighted signal response was considerably smaller using these data acquisition parameters (ranging from 20% to minus 5%) and tended to be slower, reaching statistical significance within 1 minute of switching gases in 11 of 13 HI tumors and 12 of 16 AT1s (Figs. 2-5, d-f).

Smaller HI tumors generally showed the largest BOLD response with mean signal increase ranging from 6 to 57% within 1 minute of changing gas and settling on a plateau of 4% to 66% enhancement (mean $21 \mp 7\%$, Table 1), as shown for a typical tumor (Fig. 2 a-c). The mean response of three adjacent image slices was highly consistent (Fig. 2c) and comparison of the variation of signal intensity with carbogen challenge showed no significant difference between slices (p>0.7). TOLD response was smaller and initial rapid response was followed by continued increase over 10 minutes reaching 4 to 16 % (*e.g.*, Fig. 2 d-f). Larger HI tumors showed a smaller T_2*-weighted response (Fig. 3c), but T_1-weighted response (3 to 9%) approached that of the smaller tumors (Figs. 2 & 3 f). Smaller AT1 tumors responded rapidly in both T_1- and T_2*-weighted images with little further change after 2 minutes. There was marked spatial heterogeneity with greatest response close to the tumor periphery in both T_2*- and T_1-weighted images (Fig. 4). Larger AT1 tumors showed particularly small BOLD and TOLD response (Fig. 5 c & f).

Each tumor type showed consistent responses and mean time courses are presented for both BOLD and TOLD experiments (Fig. 6 a, b) and summarized in Table 1. Noting the initial rapid dynamic response leading to stable plateau, the data in Table 1 show the mean values for SI considering only the last ten measurements during carbogen breathing. Mean changes in SI in T_1- and T_2*-weighted images of small HI tumors (reported to be well oxygenated (34, 37, 42, 43)) were significantly greater than in small or large AT1 tumors (p<0.05). The T_1-weighted image response was also significantly different between larger HI and larger AT1 tumors (Table 1).

T_2*- and T_1-weighted signal responses were well matched with a general trend of larger TOLD response being associated with larger BOLD response (Fig. 7). Considering the 29 tumors, where T_2*- and T_1-weighted signal responses were evaluated, the linear correlation coefficient $R^2>0.75$ (p<0.0001), which strengthened considerably for HI tumors alone ($R^2>0.85$; p<0.0001), although it was weaker for AT1 alone ($R^2>0.53$; p<0.002). One tumor showed particularly high values for both BOLD and TOLD responses and might be considered an outlier. If this point is neglected then the correlation for the remaining 28 tumors becomes $R^2>0.61$ (p<0.0001) and for HI alone becomes $R^2>0.59$ (p<0.005).

To investigate the origin of the changes in SI, R_1 and R_2* maps were evaluated for 27 of the tumors during air and carbogen breathing (*e.g.*, Fig. 8) and mean values are presented in Table 2. R_2* ranged from 28 to 108 s^{-1} and changed significantly for many individual

tumors, though the change was not statistically significant for any of the groups of tumors (Table 2). There was an inverse correlation between SI and R_2^* irrespective of tumor type and size ($R^2>0.48$; $p<0.0002$), which improved to $R^2>0.55$ ($p<0.002$) for AT1 tumors alone. A very similar result was observed if percentage change in R_2^* was considered in place of absolute R_2^*. Not surprisingly, R_1 and R_2^* values measured during carbogen breathing were very tightly correlated with respective baseline air breathing values, since the changes were relatively small (*e.g.*, $R_2^*_{(AT1)}$ $R^2>0.98$; $R_{1(AT1)}$ $R^2>0.938$; R_2^* $_{(HI)}$ $R^2>0.79$; $R_{1(HI)}$ $R^2>0.8$; all $p<0.001$; Fig. 8). Mean R_1 and R_2^* values were significantly different between larger HI tumors and other groups, as shown in Table 2, but none of the other groups differed significantly. Baseline R ranged from 0.389 to 0.711 s^{-1} (Table 2). If all AT1 and HI tumors are considered together then no apparent correlation was found between T_1-weighted signal and R_1 ($R^2<0.05$). Likewise for AT1 or HI tumors alone, however, if small HI tumors are considered in isolation then a strong correlation was found between T_1-weighted signal and R_1 based on absolute change in R_1 ($R^2>0.58$) or percent change in R_1 ($R^2>0.62$). A strong correlation was observed for mean R_1 vs. R_2^* in HI tumors ($R^2>0.67$; $p<0.001$), but AT1 tumors showed no obvious trend ($R^2<0.25$; Fig. 9). No significant correlations were found for either tumor type on a voxelby-voxel basis (see examples in Supplementary Data Fig. S1). Heterogeneity of baseline R_1 and R_2^* distributions, as well as response to carbogen breathing is seen in the maps (Fig. 8) and emphasized by histograms of individual voxels (Supplementary Materials, Fig. S2).

DISCUSSION

As expected, BOLD and TOLD contrast responses to breathing hyperoxic gas were quite different for the tumor sublines and sizes. Smaller HI tumors, reported to be well oxygenated and highly responsive to hyperoxic gas challenge (34, 37, 42, 43), showed the largest signal changes, whereas large AT1 tumors, reported to be hypoxic and unresponsive (33, 35, 36, 43), showed the smallest responses. Each tumor showed considerable heterogeneity within an image slice, but quite similar response between slices and overall consistency between multiple tumors of a given group.

BOLD signal responses were larger than TOLD using the current acquisition parameters, but there was a strong correlation between the magnitude of each (Fig. 7). This is reasonable since BOLD is thought to represent conversion of deoxyhemoglobin to oxyhemoglobin and additional delivery of oxygen is expected to increase pO_2. There was a general inverse trend between magnitude of BOLD signal response and change in R_2^*, but the correlation was weak. This suggests influences beyond deoxyhemoglobin concentration affected the signal intensity, which has been reported to be subject to changes in blood flow and vascular volume (24). Indeed, carbogen breathing has been reported to increase both oxyhemoglobin and total hemoglobin, as observed using near infrared spectroscopy of small HI tumors (44).

Noting that BOLD response was generally greater than TOLD response, prompts the question as to the advantage of measuring both parameters. BOLD is expected to primarily reflect vascular oxygenation, but has been reported to exhibit contradictory behavior with respect to tumor oxygenation in some cases (24, 45). Noting that TOLD responses followed BOLD (Figs. 2-6) adds confidence to the oxygen dependence, since enhanced oxygen

delivery generates elevated pO_2. In HI tumors a strong correlation was found between R_1 and R_2* (Fig. 9) consistent with change in vascular oxygenation generating change in tumor pO_2. Thus, in HI tumors TOLD may add little information regarding hypoxia and response to intervention, beyond emphasizing the BOLD response. Meanwhile, in the AT1 tumors semi quantitative BOLD and TOLD signal responses appear correlated (Fig. 7), whereas quantitative R_1 and R_2* showed distinct lack of correlation (Fig. 9). These results suggest that R_1 and R_2* may be sensitive to different biological processes emphasizing the importance of measuring both parameters and ultimately determining which may be most relevant as a prognostic biomarker for a given intervention or tumor type, as also emphasized by others (13, 32).

BOLD showed significant differences between the most responsive tumors (small HI) and small or large AT1 tumors (Table 1). By comparison TOLD showed a significant difference between the responses of larger AT1 tumors versus all the other groups. The large BOLD and TOLD responses in the HI tumors, as compared with AT1 tumors were expected, since the HI tumors are reported to be better vascularized and less hypoxic (34-36, 42, 43), as also seen in Fig. 1.

Significantly, we recently found that for a cohort of AT1 tumors, a TOLD response could be used to stratify tumors, whereby those showing a larger positive response to oxygen breathing challenge prior to single high dose radiation showed a significantly longer tumor growth delay when irradiated while breathing oxygen (33). This was not the case for BOLD response. Predictive correlation of TOLD, but not BOLD was also reported by Arias *et al*. in orthotopic C6 rat glioma with respect to single high dose radiation (46). By contrast, it has been reported that G3H prolactinomas showed a strong BOLD response to carbogen challenge, which coincided with improved tumor growth delay, while RIF-1 fibrosarcomas showed minimal response (32, 47). Baker *et al*. recently confirmed that large R_2* response in a group of G3H tumors coincided with significant reduction in hypoxia assessed using immunohistochemical markers CCI-103F and pimonidazole in a pulse chase fashion (23). For individual G3H tumors the R_2* response was quite variable, in that a large BOLD response could be associated with large or minimal change in hypoxic fraction (23); perhaps indicating that some tumors were already well oxygenated, as we believe to be the case of small HI tumors here. We previously reported that larger BOLD response coincided with elimination of hypoxic fraction in 13762NF rat breast tumors accompanying oxygen breathing (20), though we have not yet tested the radiation responsiveness in those tumors. Anecdotally, it would appear that BOLD response is relevant in well vascularized tumors (HI, GH3 and 13762NF), whereas less so in poorly vascularized tumors (RIF-1 and AT1). It will be important to evaluate the relevance of BOLD and TOLD to irradiation of HI tumors in due course.

The T_2*-weighted signal response was very similar to that reported previously for AT1 tumors (48) and baseline R_2* values fell within the range reported for diverse tumors types at 4.7 T (7, 20, 22, 47, 49). Human prostate tumors xenografts (DU145 and PC3) in mice were reported to have R_2* values and signal responses at 4.7 T similar to the R3327-AT1 and HI tumors found here (7). When tumors show a substantial BOLD response to hyperoxic gas breathing it is normally maintained until gas is returned to air (15, 17, 48).

However, a transient response was reported in PC3 tumors (7), as seen for the larger AT1 tumors here (Fig. 5c). R_1 values were in the range reported for many other tumor types at 4.7 T (50), though much lower than those reported for SCC tumors in a study of hyperoxic and hyperbaric gas intervention (29).

Semi-quantitative approaches based on change in signal intensity alone provide simple rapid indication of response to intervention (Figs. 2-7), but we recognize that the magnitude of response depends on R_1 and R_2^*, together with TE and TR times. Moreover, tumor motion sometimes precludes effective signal subtraction. Immobilizing tumors in small animals is reasonably straightforward, but in patients, respiratory or cardiac motion, or other movements such as swallowing, bladder filling and bowel peristalsis, may preclude effective signal subtraction (11). Quantitative R_1 and R_2^* measurements are slower, but even if image co-registration isn't perfect, histograms for R_1 and R_2^* distributions may be compared with respect to interventions. One might expect T_1-weighted signal response to be closely related to change in R_1, however this was only observed for the group of small HI tumors here. Various factors could be responsible for the lack of correlation; in particular the use of a spin echo acquisition protocol (SEMS) for R_1 mapping, as opposed to the SPGRE sequence for T_1 weighted imaging. The SEMS approach would be too slow for practical assessment of transient dynamics, whereas GRE provides faster time resolution. However, the two approaches are expected to experience differential sensitivity to flow effects (51). The spin echo approach using TE = 20 ms might also be biased by short T_2 water protons (*e.g.*, those near deoxygenated blood vessels that produce large magnetic field gradients).

Given that R_1 is directly dependent on pO_2 in solution, it has been suggested that changes in R_1 could directly indicate changes in tissue pO_2. Indeed in the vitreous human of the eye, a well-defined medium, Berkowitz *et al*. achieved measurements consistent with invasive electrodes (27). When we applied the calibration curve of Matsumoto *et al*. (29) to the current R_1 responses, we found general trends consistent with published ^{19}F oximetry, but also substantial discrepancies, potentially due to flow effects or temperature drift. We have recently introduced a further refinement providing quantitative oximetry based on R_1, R_2 and IVIM during air breathing (so-called MOXI) (52). However, such measurements currently require 14 minutes and make assumptions regarding oxygen hemoglobin binding and the relative amounts of oxygen carried by hemoglobin versus that dissolved in plasma, which may not be appropriate for hyperoxic gas breathing situations.

Another issue potentially confounding the use of water relaxation measurements for assessment of tumor oxygenation is the sensitivity to temperature. Sensitivity of R_1 to temperature has been reported at many magnetic fields ranging from 0.2 to 11.7 T with a general trend of decreased sensitivity at higher field (53-55). We found no data relating R_1 to temperature of aqueous solutions at 4.7 T and have undertaken a preliminary examination of an aqueous solution of Gadavist contrast agent (12.5 μM to approximately match R_1 observed for tumor). We determined a sensitivity of approximately 3% change in R_1 per degree Celsius (unpublished data). This emphasizes the importance of maintaining stable temperature during examinations of oxygen sensitive MRI, since we observed mean R_1 in the range 1.4 to 7% (Table 2), though individual tumors showed responses as large as 16% (Fig. 9). We would expect temperature variation to appear as drift rather than the acute

transition seen upon oxygen challenge (Figs. 2-5), and thus the observed changes should not be overly influenced by any temperature variations. However, changes in R_1 represent differences in maps achieved during baseline air breathing and at the end of the CB breathing period, so that temperature instability could be more significant. This should serve as a caveat for interpreting R_1 responses and may contribute to lack of correlation between % SI and R_1 in some cases.

One might expect oxygen breathing to uniformly enhance tumor oxygenation, and generate increased R_1 (induced by higher oxygen concentrations) and reduced R_2^* (induced by conversion of deoxygenation to oxyhemoglobin). In some cases we observed decreased R_1 accompanying CB breathing; notably, 6 of 13 AT1 and 2 of 13 HI tumors. Regional decrease in R_1 is noticeable in Figure 8 d and g. Negative response was extensively characterized in the recent work of Linnik *et al.* (14), who provided evidence that decreased R_1 in OE-MRI (TOLD) was spatially associated with poor perfusion (based on DCE MRI) and hypoxia (based on pimonidazole detected histologically post mortem). This is certainly consistent with the greater hypoxia often observed in AT1 tumors as compared with HI, as reported extensively (4, 33-37, 42, 43) and indicated by Figure 1.

Any new technique should be placed in the context of competing techniques (4). Many diverse approaches are available to measure pO_2 directly including invasive polarographic electrodes and fluorescent tipped fiber optic probes (15-17). Analogous measurements have been achieved using reporter molecules such as hexafluorobenzene, with ^{19}F MRI (56-58), hexamethyldisiloxane with ^{1}H MRI (59) or crystals of lithium phthalocyanine using ESR (18), based on direct injection into tissue followed by non-invasive measurement of dynamic response to interventions. Appropriate ESR and MRI reporters may be delivered systemically avoiding potential tissue damage, but potentially biasing measurements towards better perfused regions (19, 60). Hypoxia itself is widely interrogated with ^{18}F-labeled nitroimidazoles such as EF5, FAZA and F-misonidazole, but such studies involve the cost and logistic complications of handling radionuclides (61, 62). There remains debate over the optimal methodology in terms of static versus dynamic measurements and preferred timing of measurements and such reporters may not reach ischemic tissues, such as those induced by vascular disrupting agents (63). Insights into tumor oxygenation avoiding the need for reporter molecules appear particularly attractive. Near infrared spectroscopy has been used to evaluate oxy/deoxy hemoglobin ratio, though many studies have lacked spatial resolution (64, 65). In this respect photoacoustic tomography has advantages (66), although depth of signal penetration is usually limited to about 3 cm. A recent report suggests that MRI R_1 of lipids offers greater sensitivity to changes in pO_2, compared with water (67). We do note that the current study could have been strengthened if histological validation were available for each tumor, as presented by Robinson *et al.* (26) in prolactinomas and recently by Linnik *et al.* (14) for glioma on air breathing mice or Baker *et al.* (23), revealing changes in hypoxia based on pulse chase delivery of two immunohistological markers of hypoxia.

Studies comparing BOLD and TOLD in tumors have been presented in patients (glioma (13)), rabbits (VX2 (30)) and xenografts in mice (G3H and PC3 (32)). We are only aware of two previous studies in rats: Arias *et al*. (46) in glioma and our own work on AT1 tumors (33). The very different behaviors of the two syngeneic rat tumor types (AT1 and HI),

consistent with reported oximetry is potentially important and coincides with the recent study of G3H and PC3 xenografts in mice (32). Importantly, oxygen sensitive MRI is non invasive, simple to implement, highly reproducible and reveals spatial and temporal heterogeneity of oxygen dynamics. It does not quantify pO_2 or hypoxic fraction (potential advantages of ^{19}F oximetry, ESR, or electrodes (1)), but requires no needle insertion or exogenous reporter molecule beyond breathing hyperoxic. We believe evaluation of an oxygen challenge by NMR T_1 and T_2* provides a non-invasive method to distinguish between responsive and non-responsive tumors to hyperoxic gas challenge, potentially allowing hypoxic tumor identification and therapy to be tailored to these characteristics.

Supplementary Material

Refer to Web version on PubMed Central for supplementary material.

ACKNOWLEDGMENTS

Abbreviations

BOLD	blood oxygen level dependent contrast
TOLD	tissue oxygen level dependent contrast
HF	hypoxic fraction
SI	signal intensity
VDT	volume doubling time
SEMS	spin echo multiple slice
GEMS	gradient echo multiple slice
TR	repetition time
TE	echo time
FOV	field of view
CB	carbogen
ESR	electron spin resonance

References

1. Tatum JL, Kelloff GJ, Gillies RJ, Arbeit JM, Brown JM, Chao KSC, Chapman JD, Eckelman WC, Fyles AW, Giaccia AJ, Hill RP, Koch CJ, Krishna MC, Krohn KA, Lewis JS, Mason RP, Melillo G, Padhani AR, Powis G, Rajendran JG, Reba R, Robinson SP, Semenza GL, Swartz HM, Vaupel P, Yang D, Croft B, Hoffman J, Liu GY, Stone H, Sullivan D. Hypoxia: Importance in tumor biology,

noninvasive measurement by imaging, and value of its measurement in the management of cancer therapy. Int. J. Radiat. Biol. 2006; 82:699–757. [PubMed: 17118889]

2. Gray L, Conger A, Ebert M, Hornsey S, Scott O. The concentration of oxygen dissolved in tissues at time of irradiation as a factor in radiotherapy. Br. J. Radiol. 1953; 26:638–648. [PubMed: 13106296]

3. Turaka A, Buyyounouski MK, Hanlon AL, Horwitz EM, Greenberg RE, Movsas B. Hypoxic Prostate/Muscle PO_2 Ratio Predicts for Outcome in Patients With Localized Prostate Cancer: Long-Term Results. Int. J. Radiat. Oncol. Biol. Phys. 2012; 82:E433–E439. [PubMed: 21985947]

4. Mason RP, Zhao D, Pacheco-Torres J, Cui W, Kodibagkar VD, Gulaka PK, Hao G, Thorpe P, Hahn EW, Peschke P. Multimodality imaging of hypoxia in preclinical settings. QJ Nucl. Med. Mol. Imaging. 2010; 54:259–280.

5. Pacheco-Torres J, López-Larrubia P, Ballesteros P, Cerdán S. Imaging tumor hypoxia by magnetic resonance methods. NMR Biomed. 2011; 24:1–16. [PubMed: 21259366]

6. Vergis R, Corbishley CM, Norman AR, Bartlett J, Jhavar S, Borre M, Heeboll S, Horwich A, Huddart R, Khoo V, Eeles R, Cooper C, Sydes M, Dearnaley D, Parker C. Intrinsic markers of tumour hypoxia and angiogenesis in localised prostate cancer and outcome of radical treatment: a retrospective analysis of two randomised radiotherapy trials and one surgical cohort study. Lancet Oncology. 2008; 9:342–351. [PubMed: 18343725]

7. Alonzi R, Padhani AR, Maxwell RJ, Taylor NJ, Stirling JJ, Wilson JI, d'Arcy JA, Collins DJ, Saunders MI, Hoskin PJ. Carbogen breathing increases prostate cancer oxygenation: a translational MRI study in murine xenografts and humans. Br J Cancer. 2009; 100:644–648. [PubMed: 19190629]

8. Chopra S, Foltz WD, Milosevic MF, Toi A, Bristow RG, Menard C, Haider MA. Comparing oxygen-sensitive MRI (BOLD R_2*) with oxygen electrode measurements: A pilot study in men with prostate cancer. Int. J. Radiat. Biol. 2009; 85:805–813. [PubMed: 19728195]

9. Rijpkema M, Kaanders JH, Joosten FB, van der Kogel AJ, Heerschap A. Effects of breathing a hyperoxic hypercapnic gas mixture on blood oxygenation and vascularity of head-and-neck tumors as measured by magnetic resonance imaging. Int. J. Radiat. Oncol. Biol. Phys. 2002; 53:1185–1191. [PubMed: 12128119]

10. O'Connor JPB, Naish JH, Parker GJM, Waterton JC, Watson Y, Jayson GC, Buonaccorsi GA, Cheung S, Buckley DL, McGrath DM, West CML, Davidson SE, Roberts C, Mills SJ, Mitchell CL, Hope L, Ton C, Jackson A. Preliminary Study of Oxygen-Enhanced Longitudinal Relaxation in MRI: a Potential Novel Biomarker of Oxygenation Changes in Solid Tumors. Int. J. Radiat. Oncol. Biol. Phys. 2009; 75:1209–1215. [PubMed: 19327904]

11. Hallac RR, Ding Y, Yuan Q, McColl RW, Lea J, Sims RD, Weatherall PT, Mason RP. Oxygenation in cervical cancer and normal uterine cervix assessed using blood oxygenation level-dependent (BOLD) MRI at 3T. NMR Biomed. 2012; 25:1321–1330. [PubMed: 22619091]

12. Jiang L, Weatherall PT, McColl RW, Tripathy D, Mason RP. Blood oxygenation level-dependent (BOLD) contrast magnetic resonance imaging (MRI) for prediction of breast cancer chemotherapy response: A pilot study. J. Magn. Reson. Imaging. 2013; 37:1083–1092. [PubMed: 23124705]

13. Remmele S, Sprinkart AM, Muller A, Traber F, von Lehe M, Gieseke J, Flacke S, Willinek WA, Schild HH, Senegas J, Keupp J, Murtz P. Dynamic and simultaneous MR measurement of R1 and R2*changes during respiratory challenges for the assessment of blood and tissue oxygenation. Magn. Reson. Med. 2013; 70:136–146. [PubMed: 22926895]

14. Linnik IV, Scott MLJ, Holliday KF, Woodhouse N, Waterton JC, O'Connor JPB, Barjat H, Liess C, Ulloa J, Young H, Dive C, Hodgkinson CL, Ward T, Roberts D, Mills SJ, Thompson G, Buonaccorsi GA, Cheung S, Jackson A, Naish JH, Parker GJM. Noninvasive tumor hypoxia measurement using magnetic resonance imaging in murine U87 glioma xenografts and in patients with glioblastoma. Magn. Reson. Med. 2014; 71:1854–1862. [PubMed: 23798369]

15. Robinson SP, Collingridge DR, Howe FA, Rodrigues LM, Chaplin DJ, Griffiths JR. Tumor response to hypercapnia and hyperoxia monitored by FLOOD magnetic resonance imaging. NMR Biomed. 1999; 12:98–106. [PubMed: 10392806]

16. Al-Hallaq HA, River JN, Zamora M, Oikawa H, Karczmar GS. Correlation of magnetic resonance and oxygen microelectrode measurements of carbogen-induced changes in tumor oxygenation. Int. J. Radiat. Oncol. Biol. Phys. 1998; 41:151–159. [PubMed: 9588930]

17. Baudelet C, Gallez B. How does blood oxygen level-dependent (BOLD) contrast correlate with oxygen partial pressure (pO_2) inside tumors? Magn. Reson. Med. 2002; 48:980–986. [PubMed: 12465107]

18. Dunn JF, O'Hara JA, Zaim-Wadghiri Y, Lei H, Meyerand ME, Grinberg OY, Hou H, Hoopes PJ, Demidenko E, Swartz HM. Changes in oxygenation of intracranial tumors with carbogen: a BOLD MRI and EPR oximetry study. J. Magn. Reson. Imaging. 2002; 16:511–521. [PubMed: 12412027]

19. Elas M, Williams BB, Parasca A, Mailer C, Pelizzari CA, Lewis MA, River JN, Karczmar GS, Barth ED, Halpern HJ. Quantitative tumor oxymetric images from 4D electron paramagnetic resonance imaging (EPRI): Methodology and comparison with blood oxygen level-dependent (BOLD) MRI. Magn. Reson. Med. 2003; 49:682–691. [PubMed: 12652539]

20. Zhao D, Jiang L, Hahn EW, Mason RP. Comparison of ^{1}H blood oxygen level-dependent (BOLD) and ^{19}F MRI to investigate tumor oxygenation. Magn. Reson. Med. 2009; 62:357–364. [PubMed: 19526495]

21. Fan XB, River JN, Zamora M, Al-Hallaq HA, Karczmar GS. Effect of carbogen on tumor oxygenation: Combined fluorine-19 and proton MRI measurements. Int. J. Radiat. Oncol. Biol. Phys. 2002; 54:1202–1209. [PubMed: 12419449]

22. Robinson SP, Rijken PF, Howe FA, McSheehy PM, van der Sanden BP, Heerschap A, Stubbs M, Van Der Kogel AJ, Griffiths JR. Tumor vascular architecture and function evaluated by non-invasive susceptibility MRI methods and immunohistochemistry. J. Magn. Reson. Imaging. 2003; 17:445–454. [PubMed: 12655584]

23. Baker LCJ, Boult JKR, Jamin Y, Gilmour LD, Walker-Samuel S, Burrell JS, Ashcroft M, Howe FA, Griffiths JR, Raleigh JA, van der Kogel AJ, Robinson SP. Evaluation and Immunohistochemical Qualification of Carbogen-Induced R_2* as a Noninvasive Imaging Biomarker of Improved Tumor Oxygenation. Int. J. Radiat. Oncol. Biol. Phys. 2013; 87:160–167. [PubMed: 23849692]

24. Howe FA, Robinson SP, McIntyre DJO, Stubbs M, Griffiths JR. Issues in flow and oxygenation dependent contrast (FLOOD) imaging of tumours. NMR Biomed. 2001; 14:497–506. [PubMed: 11746943]

25. Baudelet C, Gallez B. Current issues in the utility of blood oxygen level dependent MRI for the assessment of modulations in tumor oxygenation. Curr Med Imaging Rev. 2005; 1:229–243.

26. Robinson SP, Rijken P, Howe FA, McSheehy PMJ, van der Sanden BPJ, Heerschap A, Stubbs M, van der Kogel AJ, Griffiths JR. Tumor vascular architecture and function evaluated by non-invasive susceptibility MRI methods and immunohistochemistry. J. Magn. Reso. Imaging. 2003; 17:445–454.

27. Berkowitz BA, McDonald C, Ito Y, Tofts PS, Latif Z, Gross J. Measuring the human retinal oxygenation response to a hyperoxic challenge using MRI: Eliminating blinking artifacts and demonstrating proof of concept. Magn. Reson. Med. 2001; 46:412–416. [PubMed: 11477648]

28. Akber SF. Correlation between oxygen tension and spin-lattice relaxation rate in tumors. Europ. J. Radiol. 1989; 9:56–59.

29. Matsumoto K, Bernardo M, Subramanian S, Choyke P, Mitchell JB, Krishna MC, Lizak MJ. MR assessment of changes of tumor in response to hyperbaric oxygen treatment. Magn. Reson. Med. 2006; 56:240–246. [PubMed: 16795082]

30. Winter JD, Akens MK, Cheng H-LM. Quantitative MRI assessment of VX2 tumour oxygenation changes in response to hyperoxia and hypercapnia. Phys. Med. Biol. 2011; 56:1225. [PubMed: 21285489]

31. O'Connor JPB, Naish JH, Jackson A, Waterton JC, Watson Y, Cheung S, Buckley DL, McGrath DM, Buonaccorsi GA, Mills SJ, Roberts C, Jayson GC, Parker GJM. Comparison of Normal Tissue R-1 and R-2* Modulation by Oxygen and Carbogen. Magn. Reson. Med. 2009; 61:75–83. [PubMed: 19097212]

32. Burrell JS, Walker-Samuel S, Baker LCJ, Boult JKR, Jamin Y, Halliday J, Waterton JC, Robinson SP. Exploring R_2* and R_1 as imaging biomarkers of tumor oxygenation. J. Magn. Reson. Imaging. 2013; 38:429–434. [PubMed: 23293077]

33. Hallac RR, Zhou H, Pidikiti R, Song K, Stojadinovic S, Zhao D, Solberg T, Peschke P, Mason RP. Correlations of noninvasive BOLD and TOLD MRI with pO$_2$ and relevance to tumor radiation response. Magn. Reson. Med. 2014; 71:1863–1873. [PubMed: 23813468]

34. Zhao D, Constantinescu A, Chang C-H, Hahn EW, Mason RP. Correlation of Tumor Oxygen Dynamics with Radiation Response of the Dunning Prostate R3327-HI Tumor. Radiat. Res. 2003; 159:621–631. [PubMed: 12710873]

35. Bourke VA, Zhao D, Gilio J, Chang C-H, Jiang L, Hahn EW, Mason RP. Correlation of Radiation Response with Tumor Oxygenation in the Dunning Prostate R3327-AT1 Tumor. Int. J. Radiat. Oncol. Biol. Phys. 2007; 67:1179–1186. [PubMed: 17336219]

36. Zhao D, Ran S, Constantinescu A, Hahn EW, Mason RP. Tumor oxygen dynamics: correlation of in vivo MRI with histological findings. Neoplasia. 2003; 5:308–318. [PubMed: 14511402]

37. Zhao D, Constantinescu C, Hahn EW, Mason RP. Differential oxygen dynamics in two diverse Dunning prostate R3327 rat tumor sublines (MAT-Lu and HI) with respect to growth and respiratory challenge. Int. J. Radiat. Oncol. Biol. Phys. 2002; 53:744–756. [PubMed: 12062621]

38. Peschke P, Hahn EW, Wenz F, Lohr F, Braunschweig F, Wolber G, Zuna I, Wannenmacher M. Differential Sensitivity of Three Sublines of the Rat Dunning Prostate Tumor System R3327 to Radiation and/or Local Tumor Hyperthermia. Radiat. Res. 1998; 150:423–430. [PubMed: 9768856]

39. Isaacs JT, Isaac WB, Feitz WFJ, Scheres J. Establishment and characterization of 7 Dunning prostate cancer cell lines and their use in developing methods for predicting metastatic ability of prostate cancer. Prostate. 1986; 9:261–281. [PubMed: 3774632]

40. Hahn EW, Peschke P, Mason RP, Babcock EE, Antich PP. Isolated tumor growth in a surgically formed skin pedicle in the rat: A new tumor model for NMR studies. Magn. Reson. Imaging. 1993; 11:1007–1017. [PubMed: 8231664]

41. Zechmann CM, Woenne EC, Brix G, Radzwill N, Ilg M, Bachert P, Peschke P, Kirsch S, Kauczor HU, Delorme S, Semmler W, Kiessling F. Impact of stroma on the growth, microcirculation, and metabolism of experimental prostate tumors. Neoplasia. 2007; 9:57–67. [PubMed: 17325744]

42. Zhao D, Constantinescu A, Hahn EW, Mason RP. Tumor oxygen dynamics with respect to growth and respiratory challenge: investigation of the Dunning prostate R3327-HI tumor. Radiat. Res. 2001; 156:510–520. [PubMed: 11604064]

43. Eble, MJ.; Wenz, F.; Bachert, KB.; Lohr, F.; Peschke, P. Invasive pO$_2$ histography in Dunning prostate tumor R-3327-AT1 and R3327-HI: Correlation with 31P-MR spectroscopy and in-vivo radiosensitivity.. In: Vaupel, PW.; Kelleher, DK.; Günderoth, M., editors. Tumor Oxygenation. Gustav Fischer; Stuttgart: 1995. p. 95-105.

44. Liu H, Gu Y, Kim JG, Mason RP. Near Infrared Spectroscopy and Imaging of Tumor Vascular Oxygenation. Methods Enzymol. 2004; 386:349–378. [PubMed: 15120261]

45. Jordan BF, Crokart N, Baudelet C, Cron GO, Ansiaux R, Gallez B. Complex relationship between changes in oxygenation status and changes in R-2(*): The case of insulin and NS-398, two inhibitors of oxygen consumption. Magn. Reson. Med. 2006; 56:637–643. [PubMed: 16897769]

46. Arias, N.; Pacheco-Torres, J.; López-Larrubia, P. Proc. Intl. Soc. Mag. Reson. Med. Vol. 20. Melbourne: 2012. Predicting response to hyperbaric oxygen radiotherapy treatment in high grade gliomas using Magnetic Resonance Imaging techniques.; p. 852

47. Rodrigues LM, Howe FA, Griffiths JR, Robinson SP. Tumor R-2 * is a prognostic indicator of acute radiotherapeutic response in rodent tumors. J. Magn. Reson. Imaging. 2004; 19:482–488. [PubMed: 15065173]

48. Jiang L, Zhao D, Constantinescu A, Mason RP. Comparison of BOLD contrast and Gd-DTPA Dynamic Contrast Enhanced imaging in rat prostate tumor. Magn. Reson. Med. 2004; 51:953–960. [PubMed: 15122677]

49. McPhail LD, Robinson SP. Intrinsic Susceptibility MR Imaging of Chemically Induced Rat Mammary Tumors: Relationship to Histologic Assessment of Hypoxia and Fibrosis. Radiology. 2010; 254:110–118. [PubMed: 20032145]

50. McSheehy PMJ, Weidensteiner C, Cannet C, Ferretti S, Laurent D, Ruetz S, Stumm M, Allegrini PR. Quantified Tumor T1 Is a Generic Early-Response Imaging Biomarker for Chemotherapy Reflecting Cell Viability. Clin. Cancer Res. 2010; 16:212–225. [PubMed: 20008843]

51. Howe FA, Robinson SP, Rodrigues LM, Griffiths JR. Flow and oxygenation dependent (FLOOD) contrast MR imaging to monitor the response of rat tumors to carbogen breathing. Magn. Reson. Imaging. 1999; 17:1307–1318. [PubMed: 10576716]

52. Zhang Z, Hallac RR, Peschke P, Mason RP. A noninvasive tumor oxygenation imaging strategy using magnetic resonance imaging of endogenous blood and tissue water. Magn. Reson. Med. 2014; 71:561–569. [PubMed: 23447121]

53. Peller M, Reinl HM, Weigel A, Meininger M, Issels RD, Reiser M. T-1 rtelaxation time at 0.2 Tesla for monitoring regional hyperthermia: Feasibility study in muscle and adipose tissue. Magn. Reson. Med. 2002; 47:1194–1201. [PubMed: 12111966]

54. Zaharchuk G, Busse RF, Rosenthal G, Manley GT, Glenn OA, Dillon WP. Noninvasive oxygen partial pressure measurement of human body fluids in vivo using magnetic resonance imaging. Acad. Radiol. 2006; 13:1016–1024. [PubMed: 16843855]

55. Lin AL, Qin Q, Zhao X, Duong TQ. Blood longitudinal (T (1)) and transverse (T (2)) relaxation time constants at 11.7 Tesla. Magn. Reson. Mat. Phys. Biol. Med. 2012; 25:245–249.

56. Zhao D, Jiang L, Mason RP. Measuring Changes in Tumor Oxygenation. Methods Enzymol. 2004; 386:378–418. [PubMed: 15120262]

57. Mignion L, Magat J, Schakman O, Marbaix E, Gallez B, Jordan BF. Hexafluorobenzene in comparison with perfluoro-15-crown-5-ether for repeated monitoring of oxygenation using ^{19}F MRI in a mouse model. Magn. Reson. Med. 2013; 69:248–254. [PubMed: 22442096]

58. Robinson SP, Griffiths JR. Current Issues in the Utility of ^{19}F Nuclear Magnetic Resonance Methodologies for the Assessment of Tumour Hypoxia. Phil. Trans Biol. Sci. 2004; 359:987–996.

59. Kodibagkar VD, Wang X, Pacheco-Torres J, Gulaka P, Mason RP. Proton Imaging of Siloxanes to map Tissue Oxygenation Levels (PISTOL): a tool for quantitative tissue oximetry. NMRBiomed. 2008; 21:899–907.

60. Mason RP, Antich PP, Babcock EE, Constantinescu A, Peschke P, Hahn EW. Non-invasive determination of tumor oxygen tension and local variation with growth. Int. J. Radiat. Oncol. Biol. Phys. 1994; 29:95–103. [PubMed: 8175452]

61. Krohn KA, Link JM, Mason RP. Molecular Imaging of Hypoxia. J. Nucl. Med. 2008; 49:129S–148S. [PubMed: 18523070]

62. Tran L-B-A, Bol A, Labar D, Jordan B, Magat J, Mignion L, Gregoire V, Gallez B. Hypoxia imaging with the nitroimidazole 18F-FAZA PET tracer: A comparison with OxyLite, EPR oximetry and 19F-MRI relaxometry. Radiother. Oncol. 2012; 105:29–35. [PubMed: 22677038]

63. Oehler C, O'Donoghue JA, Russell J, Zanzonico P, Lorenzen S, Ling CC, Carlin S. F-18-Fluromisonidazole PET Imaging as a Biomarker for the Response to 5,6-Dimethylxanthenone-4-Acetic Acid in Colorectal Xenograft Tumors. J. Nucl. Med. 2011; 52:437–444. [PubMed: 21321262]

64. Gu, Y.; Xia, M.; Liu, H.; Kodibagkar, VD.; Constantinescu, A.; Mason, RP. Biomedical Topical Meetings p. FB6, The Optical Society of America. Washington, DC: 2004. Correlation of NIR spectroscopy with BOLD MR imaging of assessing breast tumor vascular oxygen status..

65. Xia M, Kodibagkar V, Liu H, Mason RP. Tumour oxygen dynamics measured simultaneously by near infrared spectroscopy and ^{19}F magnetic resonance imaging in rats. Phys. Med. Biol. 2006; 51:45–60. [PubMed: 16357430]

66. Burton NC, Patel M, Morscher S, Driessen WHP, Claussen J, Beziere N, Jetzfellner T, Taruttis A, Razansky D, Bednar B, Ntziachristos V. Multispectral Opto-acoustic Tomography (MSOT) of the Brain and Glioblastoma Characterization. Neuroimage. 2013; 65:522–528. [PubMed: 23026761]

67. Jordan BF, Magat J, Colliez F, Ozel E, Fruytier A-C, Marchand V, Mignion L, Bouzin C, Cani PD, Vandeputte C, Feron O, Delzenne N, Himmelreich U, Denolin V, Duprez T, Gallez B. Mapping of oxygen by imaging lipids relaxation enhancement: A potential sensitive endogenous MRI contrast to map variations in tissue oxygenation. Magn. Reson. Med. 2013; 70:732–744. [PubMed: 23023932]
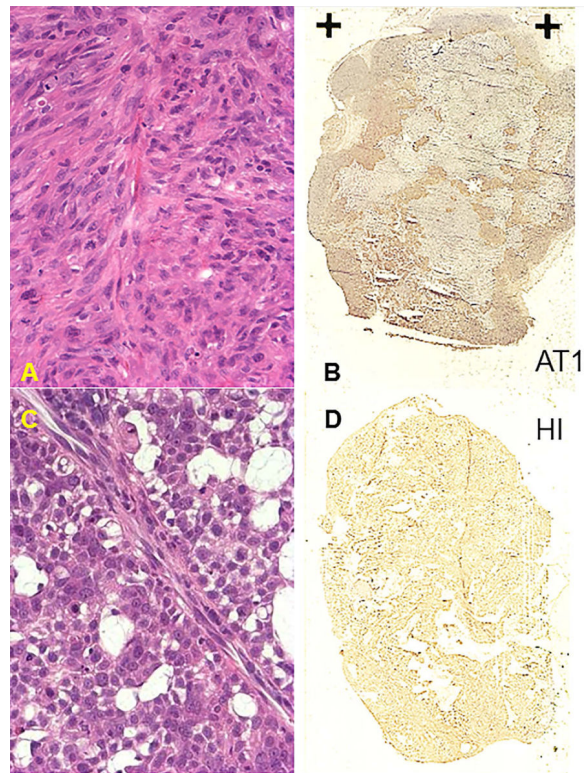
Figure 1. Histological characteristics of small Dunning prostate R3327-AT1 and -HI tumors
Upper row for AT1: A) poorly differentiated anaplastic structure is revealed by H&E; B)
widespread hypoxia in both central and peripheral regions observed using pimonidazole
(HRP-activated dark stain).

Lower row for HI: C) Moderately differentiated structures with extensive mucinous
vacuoles; D) Minimal hypoxia with just non-specific background staining. These images
show additional AT1 and HI tumors implanted specifically for histological comparison and
do not correspond to any of the imaged animals.
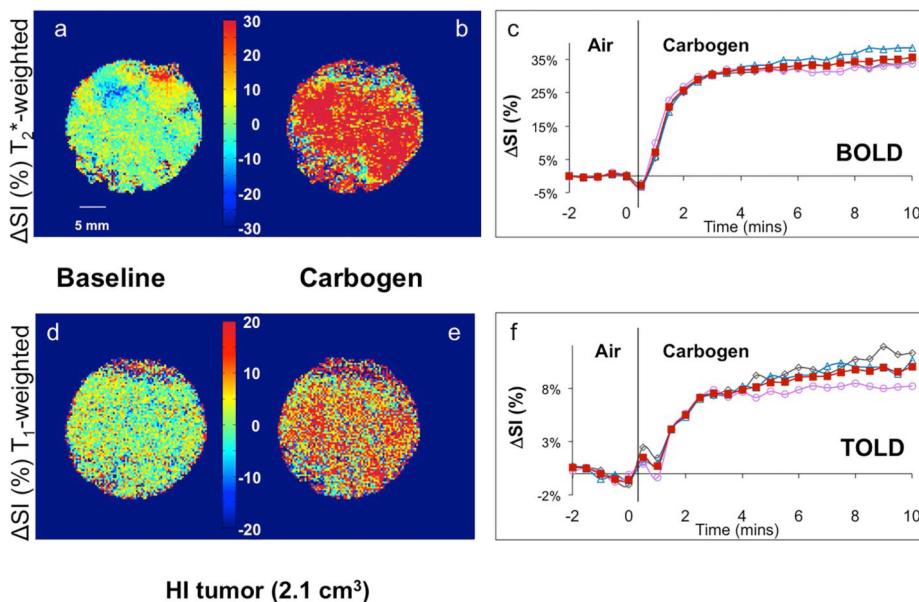
Figure 2. Response of T_1- and T_2*-weighted image signal intensity to carbogen challenge in a small Dunning prostate R3327-HI tumor (2.1 cm^3)

Normalized spin echo planar T_2*-weighted cross-sectional images of the tumor acquired while breathing (a) air (baseline), and (b) carbogen (image selected to show maximum change), c) Mean BOLD (normalized signal intensity (SI)) response in three adjacent image slices ($\bigcirc$, $\triangle$, $\diamond$) and mean over whole tumor ($\blacksquare$). Corresponding normalized T_1-weighted gradient echo images of the tumor acquired breathing (d) air and (e) carbogen. f) Mean variations across the tumor of normalized SI change vs. time (TOLD response). Heat scale bar shows % change and linear scale = 5 mm.
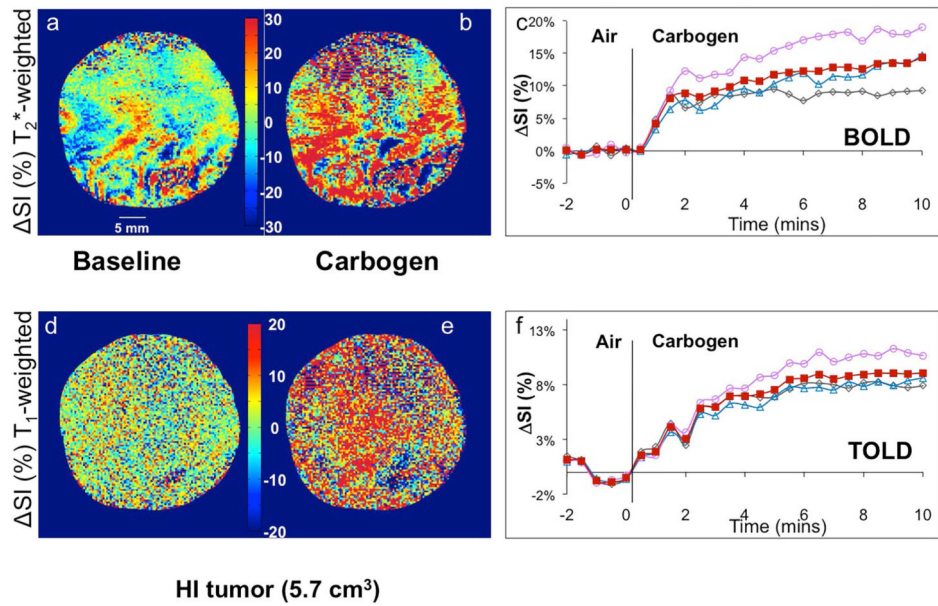
HI tumor (5.7 cm³)

Figure 3. Signal response to carbogen challenge in a large Dunning prostate R3327-HI tumor
Data correspond to Figure 2, but for a larger HI tumor (5.7 cm³). The BOLD response was significant, but considerably less than in the smaller HI tumor, whereas TOLD response was quite similar to smaller tumors.
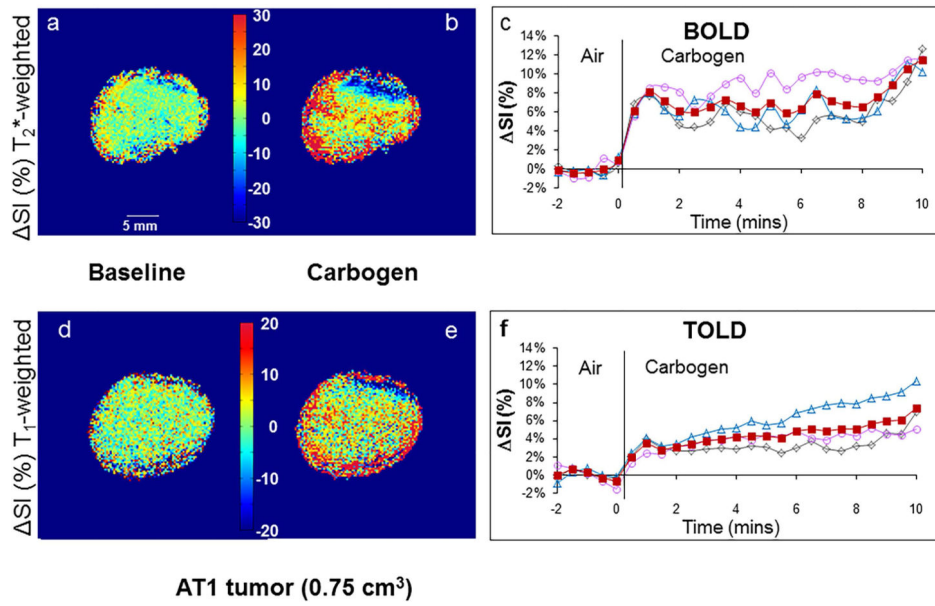
AT1 tumor (0.75 cm³)

Figure 4. Signal response to carbogen challenge in small R3327-AT1 tumor
Data correspond to Figure 2, but in a small AT1 tumor (0.75 cm³). The BOLD and TOLD responses were each considerably less than in the small HI tumor.
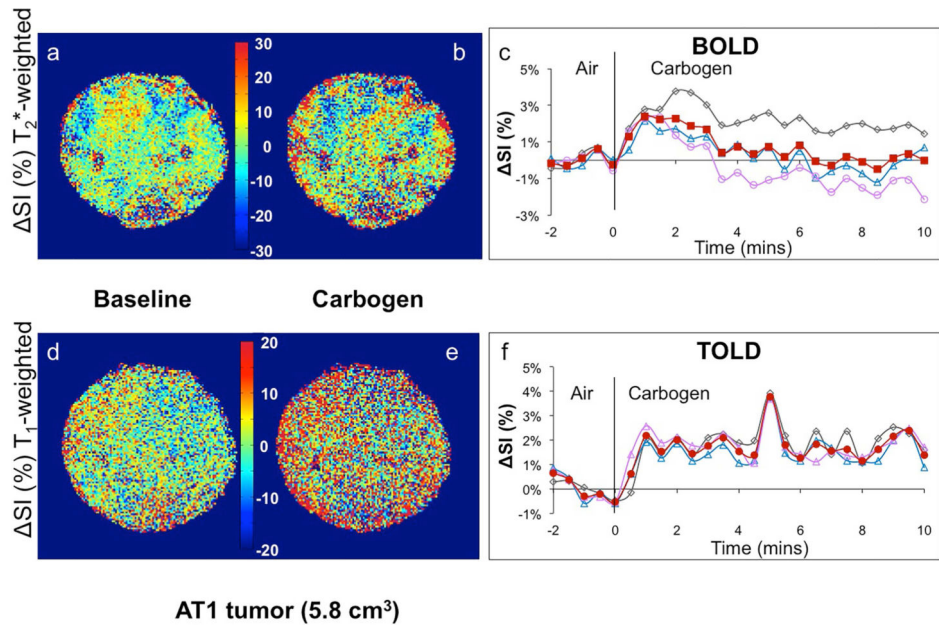
AT1 tumor (5.8 cm³)

Figure 5. Signal response to carbogen challenge in a large R3327-AT1 tumor
Data correspond to Figure 2, but in a larger AT1 tumor (5.8 cm³). The BOLD and TOLD responses were each considerably smaller than in the other tumors.
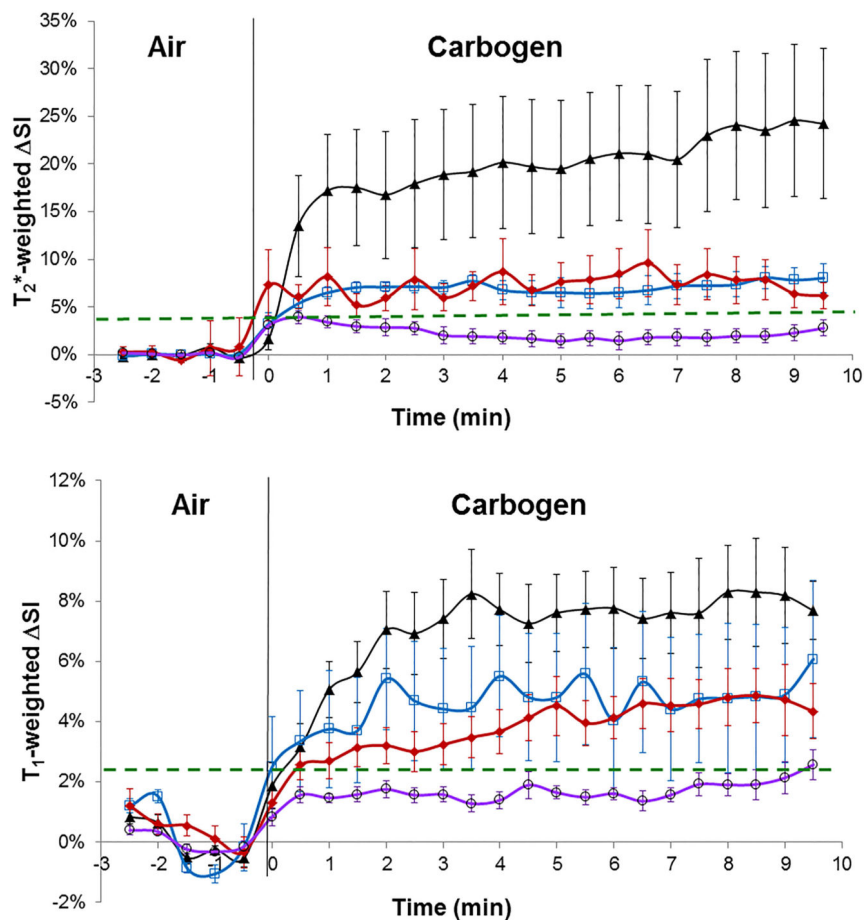
Figure 6. Comparison of BOLD and TOLD response in groups of Dunning prostate tumors

a. Dynamic normalized T_2*-weighted signal response to carbogen challenge in the four different groups of tumors. ▲ (smaller HI; n= 8), ◆ (smaller AT1; n= 9), □ (larger HI; n= 5), ○ (larger AT1; n= 7), showing mean ± SEM.

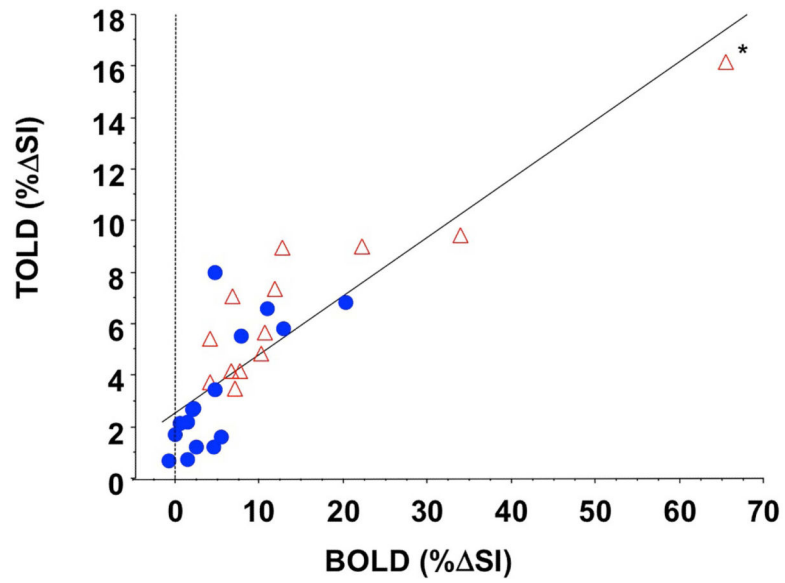**b.** Corresponding T_1-weighted signal responses.

Figure 7. Correlation of TOLD and BOLD response to carbogen challenge
Signal enhancement showed a distinct linear correlation for all tumors (n=29) from this study (red and blue symbols; $R^2 > 0.75$; $p < 0.0001$). HI tumors (open red triangles) alone showed even stronger correlation ($R^2 > 0.85$; $p < 0.0001$). AT1 tumors from this study (blue circles) showed a somewhat weaker correlation ($R^2 > 0.54$; $p < 0.005$).
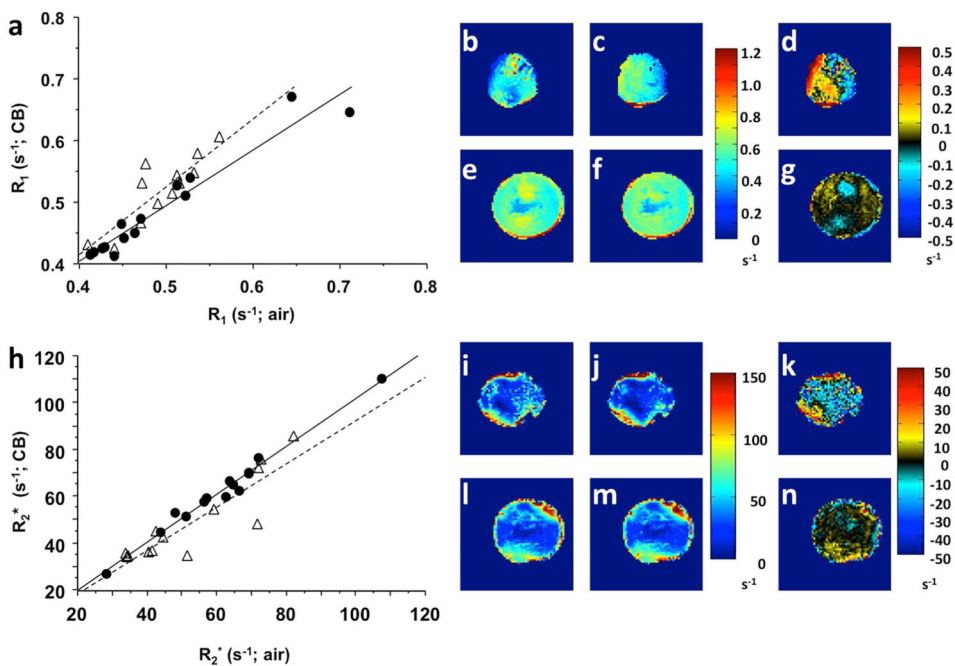
Figure 8. Influence of carbogen challenge on R_1 and R_2*

Groups of AT1 (●) and HI (△) tumors are shown separately with respect to carbogen gas breathing challenge. a) a strong correlation was observed between baseline R and that measured during carbogen breathing with $R^2 = 0.802$ (HI) and $R^2 = 0.936$ (AT1). b) R_1 map for a slice through a small HI tumor, revealing baseline spatial heterogeneity. c) corresponding R_1 map with CB breathing; d) difference map showing response to CB challenge; e) baseline R_1 map for large AT1 tumor; f) corresponding R_1 map with CB; g) difference map showing small response in large AT1 tumor. Corresponding R_2* data with tumors matching those in a-g; h) Correlations were quite similar for R_2* ($R^2 = 0.798$ (HI); $R^2 = 0.981$ (AT1)), as expected since the changes in each relaxation rate was relatively small. i) baseline R_2* small HI; j) R_2* (CB) small HI; k) R_2* difference small HI; l) baseline R_2* big AT1; m) R_2* CB big AT1; n) △R_2* big AT1.
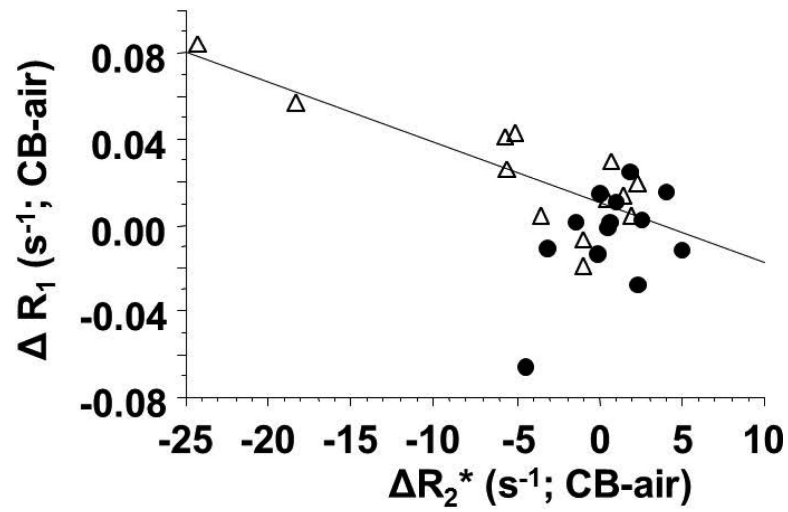
Figure 9. Correlation of quantitative TOLD and BOLD response to carbogen challenge
Comparison of AT1 (●) and HI (△) tumors showed distinct trends for the group of 29 tumors. Mean change in R_1 was closely reflective of R_2^* for HI tumors (linear fit shown, $R^2 > 0.67$), but there was no obvious relationship for the AT1 tumors.

Table 1

T_2*- (BOLD) and T_1- (TOLD) weighted signal response to carbogen challenge in groups of Dunning prostate R3327 tumors

Tumor	BOLD (% SI) range	TOLD (% SI) range
Smaller HI (n=8)	21 ± 7^a 4-66%	8 ± 1 4-16%
Smaller AT1 (n=9)	8 ± 2 0.6-20%	4.5 ± 0.9 1-8%
Larger HI (n=5[c])	7 ± 1 4-13%	5 ± 1 3-9%
Larger AT1 (n=7)	1.8 ± 0.8 −0.6-5.6%	1.9 ± 0.3^b 0.7-2.7%

[a] $p < 0.05$ versus smaller and larger AT1

[b] versus smaller AT1 and small or large HI

[c] BOLD and TOLD data available for 5 of 9 large HI tumors.

Table 2

Mean relaxation rates, R_1 and R_2*, in groups of tumors with respect to carbogen breathing challenge

Tumor (n)	R_2* air (s^{-1})	R_2* CB (s^{-1})	R_2* (s^{-1})	R_1 air (s^{-1})	R_1 CB (s^{-1})	R_1 (s^{-1})
HI (smaller) (5)	66 ± 6^d 72.5 (45-82)	65 ± 8^d 71.8 (42-85)	−1.0	0.45 ± 0.02 0.442 (0.389-0.514)	0.46 ± 0.02^d 0.430 (0.413-0.512)	0.007
HI (larger) (8)	44 ± 4 41.3 (34-72)	37 ± 2 35.5 (34-48)	−5.5	0.51 ± 0.01 0.515 (0.472-0.563)	0.54 ± 0.01 0.544 (0.464-0.605)	0.033
AT1 (smaller) (8)	64 ± 8^d 64.6 (28-108)	64 ± 8^d 61.0 (27-110)	−0.1	0.52 ± 0.04 0.468 (0.440-0.711)	0.51 ± 0.03 0.469 (0.412-0.671)	$−0.007^d$
AT1* (larger) (6)	58 ± 5 59.9 (44-69)	59 ± 4^d 61.0 (44-70)	1.6^d	0.46 ± 0.02 0.428 (0.413-0.528)	0.46 ± 0.03 0.426 (0.415-0.539)	0.000^d

($R = R_{CB} - R_{air}$); data presented as mean ± se, followed by median and range in parentheses; (n) represents number of tumors with R_1 and R_2* data available

[d] $p<0.05$ vs. larger HI tumors (Fisher's PLSD using ANOVA).